Supporting Information

Nanochannel-Confined Graphene Quantum Dots for Ultrasensitive Electrochemical Analysis of Complex Samples

Lili Lu[†,1] *Lin Zhou*[†,1] *Jie Chen,*[2] *Fei Yan,*[1] *Jiyang Liu,*[*,1] *Xiaoping Dong,*[1] *Fengna Xi,*[1] *Peng Chen*[*,2]

[1] Department of Chemistry, Zhejiang Sci-Tech University, 928 Second Avenue, Xiasha Higher Education Zone, Hangzhou, 310018, PR China.

[2] School of Chemical & Biomedical Engineering, Nanyang Technological University, 70 Nanyang Drive, Singapore 637457

[†]These authors contributed equally to this work.

S1. Characterization of the functional groups and surface charge of OH-GQDs.

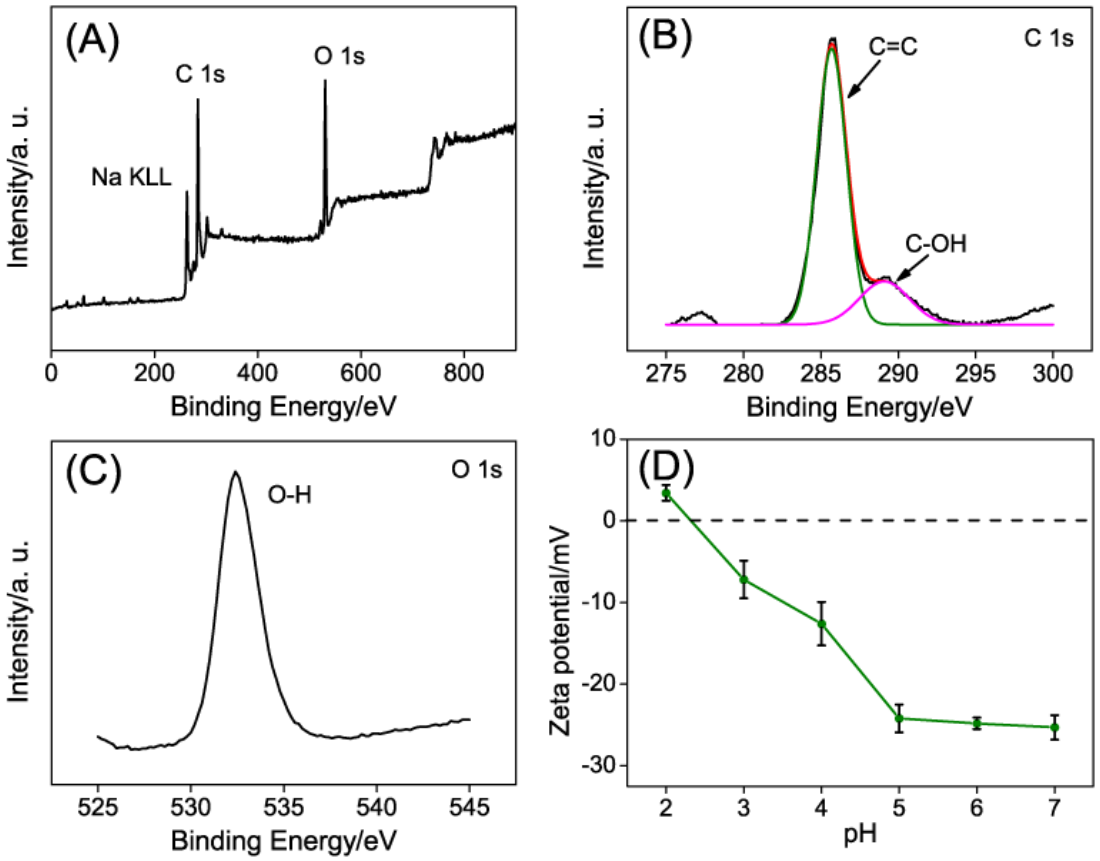

Figure S1. X-ray photoelectron spectroscopy (XPS) survey spectrum (A) and high-resolution C1s (B), O1s (C) spectra of OH-GQDs. (D) Zeta potential of OH-GQDs at different pH.

S2. Characterization of the selectivity and size change of OH-GQDs towards metal ions .

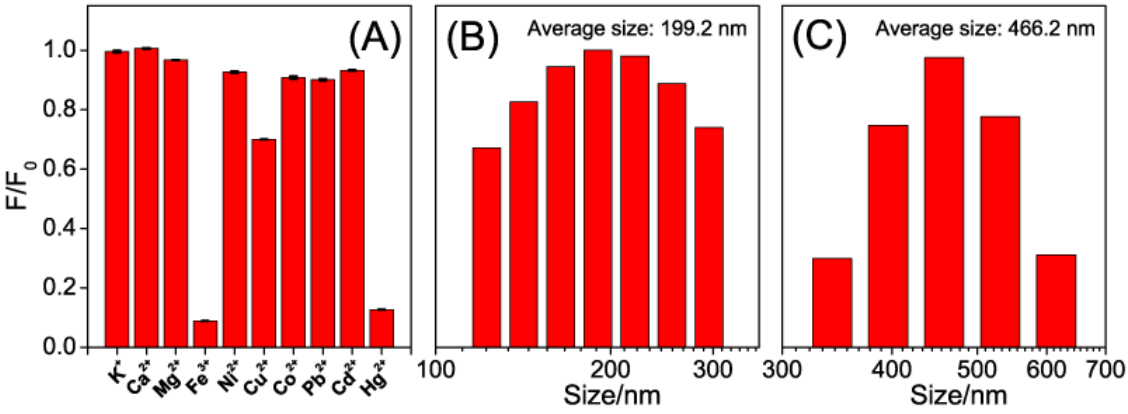

Figure S2. (A) The fluorescence intensity ratio obtained from OH-GQDs in the absence (F_0) and presence (F) of various metal ions (0.5 mM). (B-C) The dynamic light scattering (DLS) of OH-GQDs in the presence of 0.1 mM of Cu^{2+} (B) or Hg^{2+} (C), respectively.

S3. Characterization of morphology, composition, surface charge and selectivity of NH_2-GQDs.

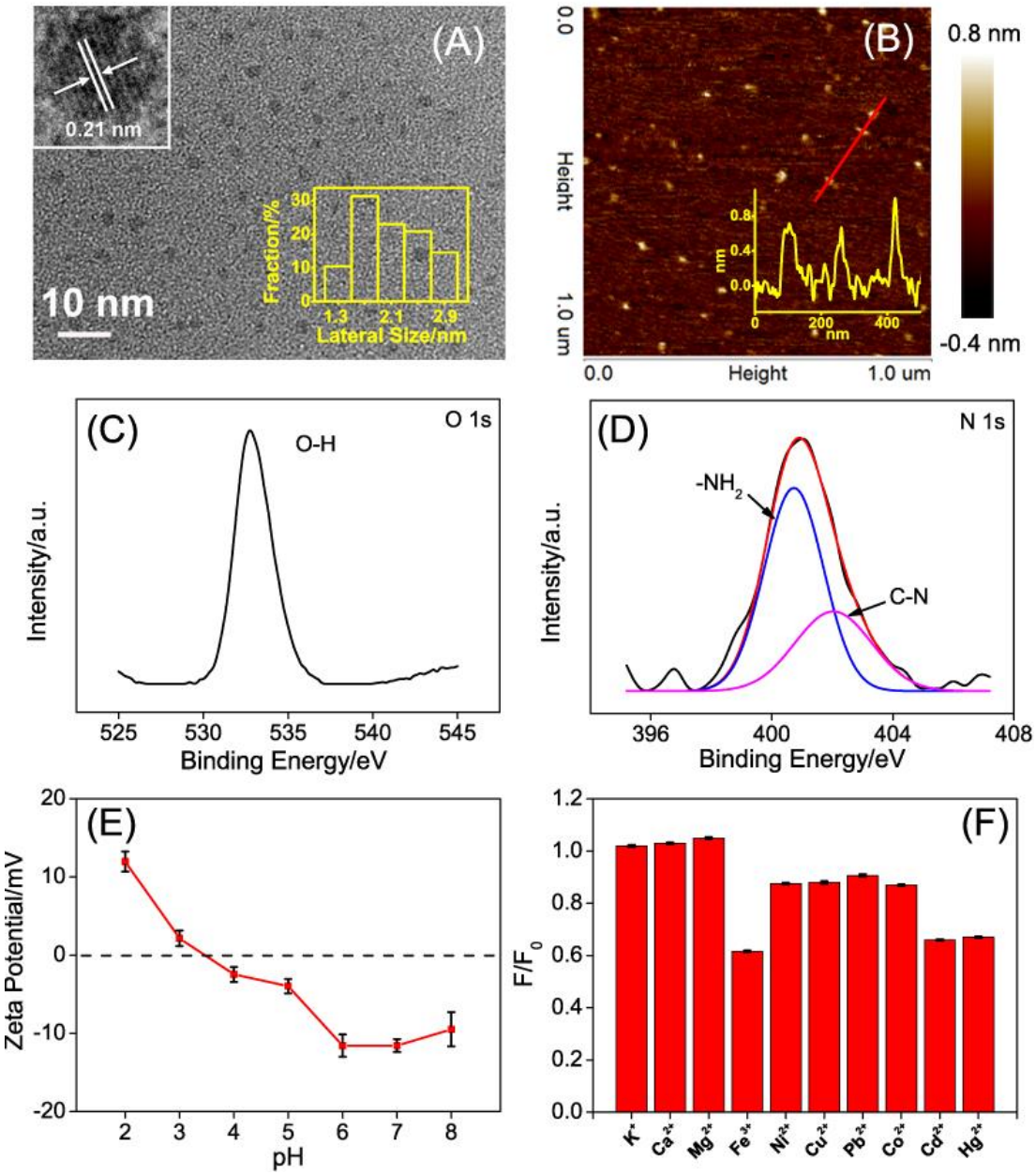

Figure S3. TEM images of NH_2-GQDs. Insets present high-resolution TEM (HRTEM) image with resolved crystalline lattice (left) and size distribution of 89 NH_2-GQDs (right). (B) AFM image of NH_2-GQDs. Inset is the height profile along the indicated red line. (C-D) High-resolution XPS O1s and N1s spectra of NH_2-GQDs. (E) Zeta potential of NH_2-GQDs at different pH. (F) The fluorescent intensity ratio obtained from NH_2-GQDs in the absence (F_0) and presence (F) of various metal ions (0.5 mM).

S4. Electrochemical characterization of OH-GQD@VMSF/ITO or NH_2-GQD@VMSF/ITO.

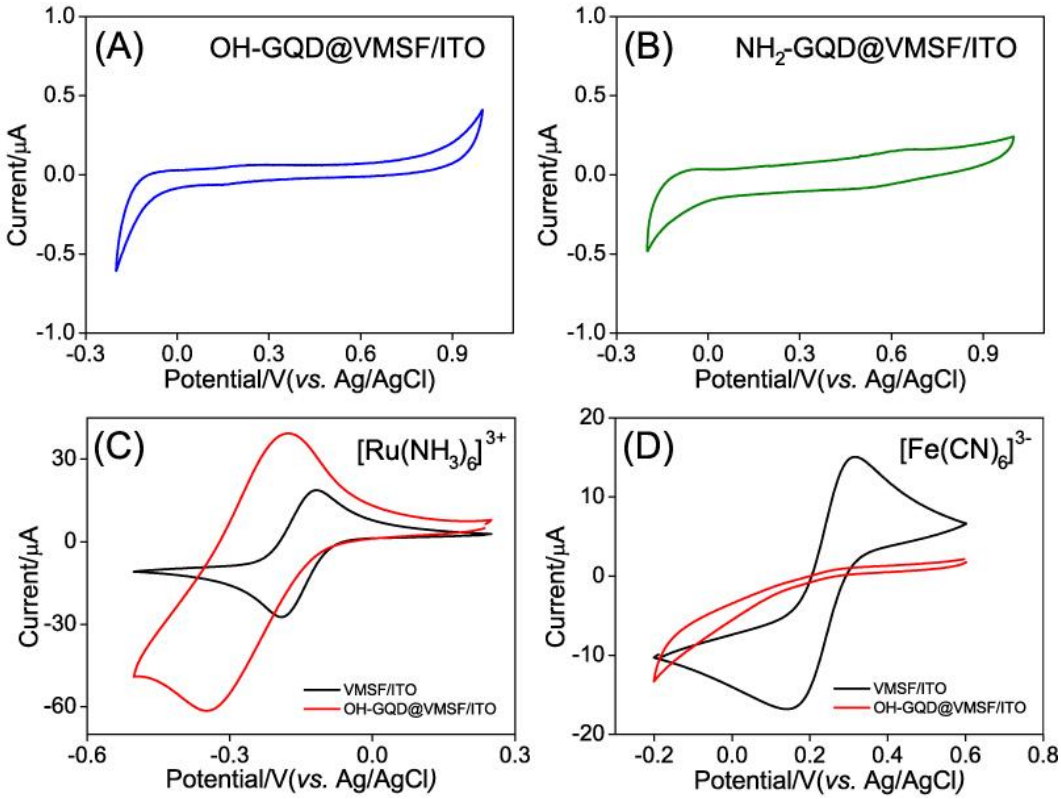

Figure S4. (A-B) Cyclic voltammetry (CV) curves obtained from OH-GQD@VMSF/ITO or NH_2-GQD@VMSF/ITO electrode in 0.1 M PBS solution (pH 6.8). (C-D) CV curves obtained from VMSF/ITO or OH-GQD@VMSF/ITO electrodes in 0.5 mM of $Ru(NH_3)_6^{3+}$ (C) or $Fe(CN)_6^{3-}$ (D).

S5. The effects of pH and electrodeposition time on the detection of metal ions.

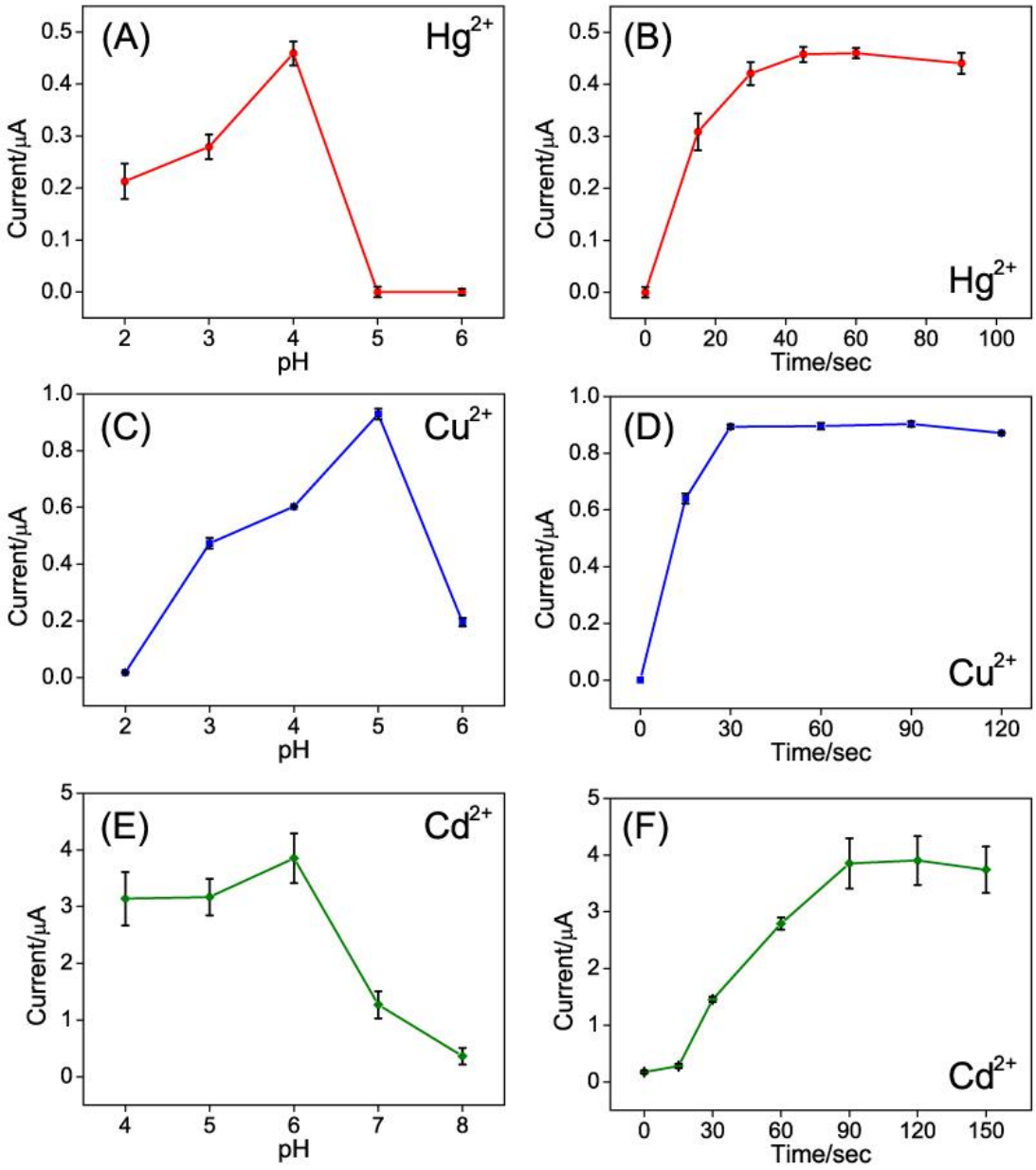

Figure S5. The effects of pH and electrodeposition time on detection of Hg^{2+} (A-B, 0.1 μM), Cu^{2+} (C-D, 1μM) or Cd^{2+} (E-F, 1μM).

S6. Detection of Hg^{2+} or Cu^{2+} or Cd^{2+} at high concentrations using GQD@VMSF/ITO electrode.

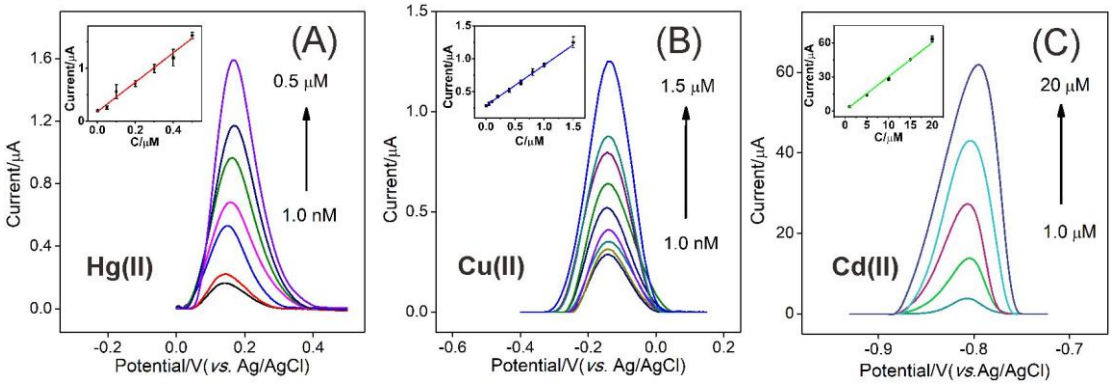

Figure S6. (A-B) Differential pulse voltammetry (DPV) curves obtained from OH-GQD@VMSF/ITO electrode in response to different concentrations of Hg^{2+} or Cu^{2+}. (C) DPV curves obtained from NH_2-GQD@VMSF/ITO electrode in response to different concentrations of Cd^{2+}. The insets in A-C show the linear dose response curves in the high concentration range.

S7. Simultaneous detection of Hg^{2+} and Cu^{2+} using OH-GQD@VMSF/ITO electrode.

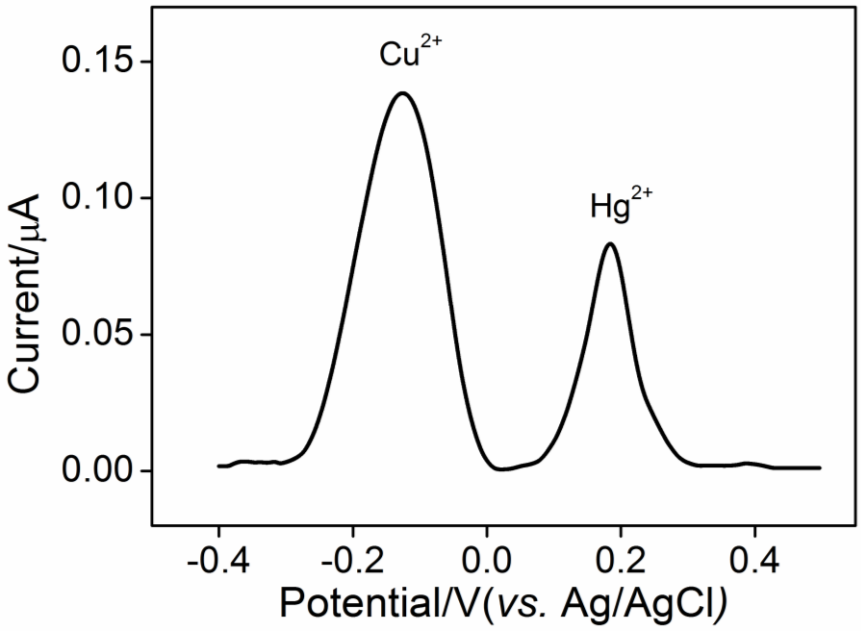

Figure S7. DPV curve obtained from OH-GQD@VMSF/ITO electrode in response to Hg^{2+} (0.25 nM) and Cu^{2+} (0.6 nM).

S8. The anti-fouling and anti-interference properties of GQD@VMSF/ITO for the detection of Hg^{2+} or Cu^{2+}or Cd^{2+}.

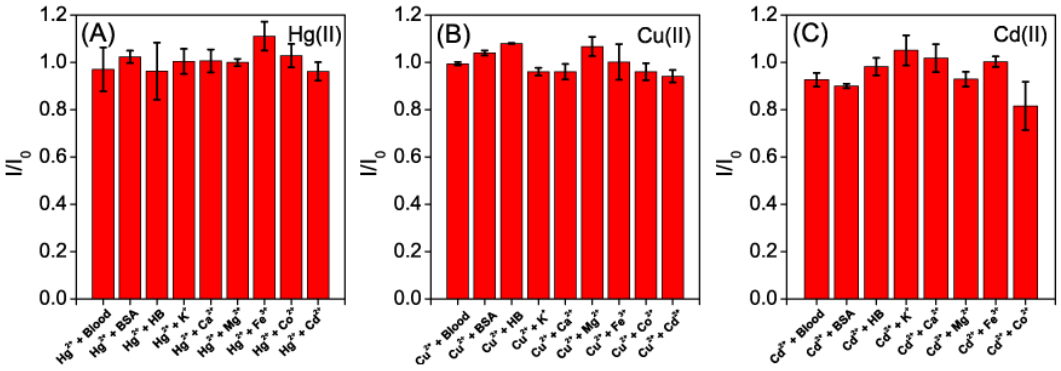

Figure S8. (A-B) The current ratio obtained from OH-GQD@VMSF/ITO in Hg^{2+} or Cu^{2+} solution containing different substances. (C) The current ratio obtained from NH_2-GQD@VMSF/ITO in Cd^{2+} solution containing different substances. The concentration of Hg^{2+}, Cu^{2+} or Cd^{2+} is 0.5 μM. The concentrations of other metal ions or substrates are 5.0 μM or 20.0 μg/mL, respectively. The human blood was diluted by a factor of 100.

S9. Characterization of morphology of VMSF prepared by EASA method on Au electrode.

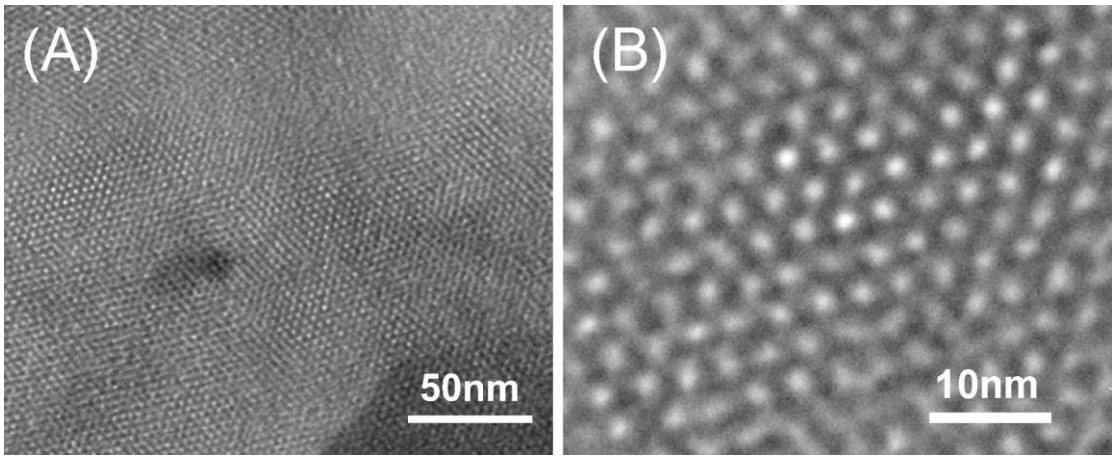

Figure S9. (A and B) Top-view TEM images of VMSF prepared by the EASA method on Au electrode.

S10. Detection performance of different electrochemical sensors.

.

Table S1 Comparison between electrochemical detection of Cd^{2+}, Cu^{2+} and Hg^{2+} using different modified electrode.

Electrode materials	***Analyte***	***Detection range***	***LOD***	*Ref.*
GQD@VMSF/ITO	Hg^{2+}; Cu^{2+}; Cd^{2+}	10 pM-1 nM; 10 pM-1 nM; 20 nM-1.0 μM	9.8 pM; 8.3 pM; 4.3 nM	This work
$NiCo_2O_4$ nanoplatelets/GCE	Hg^{2+}; Cu^{2+}; Cd^{2+}	0.8-2.0 μM; 0.1-1.0 μM; 0.1-1.0 μM	42.9 nM; 29.5 nM; 40 nM	1
C_{60}-CS/GCE	Hg^{2+}; Cu^{2+}; Cd^{2+}	0.01-6.0 μM; 0.05-6.0 μM; 0.5-9.0 μM	3 nM; 14 nM; 21 nM	2
Alk-Ti_3C_2/GCE	Hg^{2+}; Cu^{2+}; Cd^{2+}	0.1-1.5 μM; 0.1-1.5 μM; 0.1-1.5 μM	130 nM; 32 nM; 98 nM	3
IAP30/RTIL electrode	Hg^{2+}; Cu^{2+}; Cd^{2+}	0.3-1.3 μM; 0.1-2.5 μM; 0.1-2.5 μM	0.6 nM; 2 nM; 8 nM	4
Fe_3O_4/GO- PtNAs/CF	Hg^{2+}	0.1 nM-100 nM	30 pM	5
Fe_3O_4@AuNPs-DNA	Hg^{2+}	10-100 nM	1.7 nM	6
MCH/P1/Au_{plate}/GCE	Hg^{2+}	0.1 nM-250 μM	0.01 nM	7
porous 3D S-doped RGO	Hg^{2+}	0-0.6 μM	0.5 nM	8
DSP-AuNPs/PAMAM/MWCNT/GCE	Cu^{2+}	0.001-1 μM	0.48 nM	9
GQDs/graphene/ GCE	Cu^{2+}	0.015-8.775 μM	1.34 nM	10
GCE/PAA	Cu^{2+}	0.050-10 μM	8.4 nM	11
Lab-on-a-tip gold wires	Cu^{2+}	0.3-4.7 μM	94. 4 nM	12
ePAD with IS film electrodes	Cd^{2+}	0.044-0.356 μM	8.0 nM	13
NCQDs-GO/GCE	Cd^{2+}	0.1-100 μM	66. 2 nM	14
Nano Al_4SiC_4-RGO/GCE	Cd^{2+}	0.45-24.0 μM	19 nM	15
Nano NH_2/SnO_2-RTL/ GCE	Cd^{2+}	0.01-0.2 μM	5.4 nM	16
Gold-coated nano carbon tape	Cd^{2+}	0.018-1.33 nM	0.9 nM	17

GCE, glassy carbon electrode; C_{60}-CS, C_{60}-Chitosan; Alk-Ti_3C_2, alkaline intercalated Ti_3C_2 Mxene; IAP30, irradiated attapulgite; RTIL, ionic liquid composites; RGO, reduced graphene oxide; PtNAs/CF, platinum nanotube arrays modified carbon fibers; Fe_3O_4@AuNPs-DNA, DNA modified Fe_3O_4@Au magnetic nanoparticles; MCH/P1/Au_{plate}, 6-mercaptohexanol/thiolated capture probe/Au-plated; DSP-AuNPs/PAMAM/MWCNT, dithiobis[succinimidylpropionate] encapsulated Au nanoparticles/poly(amidoamine) dendrimers/multi-walled carbon nanotubes; PAA, poly(azure A); ePAD with IS film, electrochemical paper-based analytical device with integrated sputtered film; NCQDs, N-doped carbon quantum dots.

References

(1) Liao, J.; Zhang, J.; Wang, C. Z.; Lin, S., Electrochemical and Density Functional Theory Investigation on The Differential Behaviors of Core-Ring Structured $NiCo_2O_4$ Nanoplatelets toward Heavy Metal Ions. *Anal. Chim. Acta* **2018**, *1022*, 37-44.
(2) Han, X.; Meng, Z.; Zhang, H.; Zheng, J., Fullerene-Based Anodic Stripping Voltammetry for Simultaneous Determination of Hg(II), Cu(II), Pb(II) and Cd(II) in Foodstuff. *Microchim. Acta* **2018**, *185*, 274.
(3) Zhu, X.; Liu, B.; Hou, H.; Huang, Z.; Zeinu, K. M.; Huang, L.; Yuan, X.; Guo, D.; Hu, J.; Yang, J., Alkaline Intercalation of Ti_3C_2 MXene for Simultaneous Electrochemical Detection of Cd(II), Pb(II), Cu(II) and Hg(II). *Electrochim. Acta* **2017**, *248*, 46-57.
(4) Xiong, S.; Xu, J.; Xie, F.; Hu, X.; Gong, G.; Wu, Z.; Yao, L., Stripping Analysis of Pb(II), Cd(II), Hg(II) and Cu(II) Based on Irradiated Attapulgite/Ionic Liquid Composites. *Chem. Eng. J.* **2017**, *316*, 383-392.
(5) Luo, J.; Jiang, D.; Liu, T.; Peng, J.; Chu, Z.; Jin, W., High-Performance Electrochemical Mercury Aptasensor Based on Synergistic Amplification of Pt Nanotube Arrays and Fe_3O_4 /rGO Nanoprobes. *Biosens. Bioelectron.* **2018**, *104*, 1-7.
(6) Miao, P.; Tang, Y.; Wang, L., DNA Modified Fe_3O_4@Au Magnetic Nanoparticles as Selective Probes for Simultaneous Detection of Heavy Metal Ions. *ACS Appl. Mater. Interfaces* **2017**, *9*, 3940-3947.
(7) Xu, A.; Chao, L.; Xiao, H.; Sui, Y.; Liu, J.; Xie, Q.; Yao, S., Ultrasensitive Electrochemical Sensing of Hg^{2+} Based on Thymine-Hg^{2+}-Thymine Interaction and Signal Amplification of Alkaline Phosphatase Catalyzed Silver Deposition. *Biosens. Bioelectron.* **2018**, *104*, 95-101.
(8) Manna, B.; Raj, C. R., Nanostructured Sulfur-Doped Porous Reduced Graphene Oxide for the Ultrasensitive Electrochemical Detection and Efficient Removal of Hg(II). *ACS Sustainable Chem. Eng.* **2018**, *6*, 6175-6182.
(9) Cui, L.; Wu, J.; Li, J.; Ge, Y.; Ju, H., Electrochemical Detection of Cu^{2+} through Ag Nanoparticle Assembly Regulated by Copper-Catalyzed Oxidation of Cysteamine. *Biosens. Bioelectron.* **2014**, *55*, 272-277.
(10) Wang, Y.; Zhao, S.; Li, M.; Li, W.; Zhao, Y.; Qi, J.; Cui, X., Graphene Quantum Dots Decorated Graphene as An Enhanced Sensing Platform for Sensitive and Selective Detection Of Copper(II). *J. Electroanal. Chem.* **2017**, *797*, 113-120.
(11) Liu, T.; Luo, Y.; Kong, L.; Zhu, J.; Wang, W.; Tan, L., Voltammetric Detection of Cu^{2+} using Poly(azure A) Modified Glassy Carbon Electrode Based on Mimic Peroxidase Behavior of Copper. *Sens. Actuators, B* **2016**, *235*, 568-574.
(12) Cinti, S.; Mazzaracchio, V.; Ozturk, G.; Moscone, D.; Arduini, F., A Lab-On-A-Tip Approach to Make Electroanalysis User-Friendly and Decentralized: Detection of Copper Ions in River Water. *Anal. Chim. Acta* **2018**, *1029*, 1-7.
(13) Kokkinos, C.; Economou, A.; Giokas, D., Paper-Based Device with a Sputtered Tin-Film Electrode for the Voltammetric Determination of Cd(II) and Zn(II). *Sens. Actuators, B* **2018**, *260*, 223-226.
(14) Li, L.; Liu, D.; Shi, A.; You, T., Simultaneous Stripping Determination of Cadmium and Lead Ions Based on the N-Doped Carbon Quantum Dots-Graphene Oxide Hybrid. *Sens. Actuators, B* **2018**, *255*, 1762-1770.
(15) Wu, Y.; Yang, T.; Chou, K. C.; Chen, J.; Su, L.; Hou, X., The Effective Determination of Cd(II) and Pb(II) Simultaneously Based on An Aluminum Silicon Carbide-Reduced Graphene Oxide Nanocomposite Electrode. *Analyst* **2017**, *142*, 2741-2747.
(16) Yang, M.; Jiang, T.-J.; Guo, Z.; Liu, J.-H.; Sun, Y.-F.; Chen, X.; Huang, X.-J., Sensitivity and Selectivity Sensing Cadmium(II) Using Amination Functionalized Porous SnO_2 Nanowire Bundles-Room Temperature Ionic Liquid Nanocomposite: Combined Efficient

Cation Capture with Control Experimental Conditions. *Sens. Actuators, B* **2017**, *240*, 887-894.
(17) Bi, X.-M.; Wang, H.-R.; Ge, L.-Q.; Zhou, D.-M.; Xu, J.-Z.; Gu, H.-Y.; Bao, N., Gold-Coated Nanostructured Carbon Tape for Rapid Electrochemical Detection of Cadmium in Rice with In Situ Electrodeposition of Bismuth in Paper-Based Analytical Devices. *Sens. Actuators, B* **2018**, *260*, 475-479.